Author Manuscript

Author Manuscript

Author Manuscript

Author Manuscript

HHS Public Access

Author manuscript

DNA Repair (Amst). Author manuscript; available in PMC 2021 January 01.

Published in final edited form as:

DNA Repair (Amst). 2020 January ; 85: 102747. doi:10.1016/j.dnarep.2019.102747.

Novel Deazaflavin Tyrosyl-DNA Phosphodiesterase 2 (TDP2) Inhibitors

Evgeny Kiselev[a], **Azhar Ravji**[a], **Jayakanth Kankanala**[b], **Jiashu Xie**[b], **Zhengqiang Wang**[b], **Yves Pommier**[a]

[a]Developmental Therapeutics Branch and Laboratory of Molecular Pharmacology, Center for Cancer Research, National Cancer Institute, National Institutes of Health, Bethesda, MD 20892, United States.

[b]Center for Drug Design, College of Pharmacy, University of Minnesota, Minneapolis, MN 55455, United States.

Abstract

Tyrosyl-DNA phosphodiesterase 2 (TDP2) is a DNA repair enzyme that removes 5′-phosphotyrosyl blockages resulting from topoisomerase II (TOP2)-DNA cleavage complexes trapped by TOP2 inhibitors. TDP2 is a logical target for the development of therapeutics to complement existing treatments based on inhibition of TOP2. There is, however, no TDP2 inhibitor in clinical development at present. Of the reported TDP2 inhibitors, the deazaflavins are the most promising chemical class centered around the lead compound SV-5-153. Recently we reported new subtypes derived within the deazaflavin family with improved membrane permeability properties. In this work we characterize two representative analogues from two new deazaflavin subtypes based on their biochemical TDP2 inhibitory potency and drug-likeness. We demonstrate that the ZW-1288 derivative represents a promising direction for the development of deazaflavins as therapeutic agents. ZW-1288 exhibits potent inhibitory activity at low nanomolar concentrations against recombinant and cellular human TDP2 with profile similar to that of the parent analog SV-5-153 based on high resistance against murine TDP2 and human TDP2 mutated at residue L313H. While expressing weak cytotoxicity on its own, ZW-1288 potentiates the clinical TOP2 inhibitors etoposide (ETP) and mitoxantrone in human prostate DU145 and CCRF-CEM leukemia and chicken lymphoma DT40 cells while not impacting the activity of the topoisomerase I (TOP1) inhibitor camptothecin or the PARP inhibitor olaparib. ZW-1288 increases the uptake of ETP to a lesser extent than SV-5-153 and remained active in TDP2 knockout cells indicating that the deazaflavin TDP2 inhibitors have additional cellular effects that will have to be taken into account for their further development as TDP2 inhibitors.

Keywords

Tyrosyl-DNA phosphodiesterase; deazaflavin; topoisomerase; etoposide; mitoxantrone; inhibitor

Publisher's Disclaimer: This is a PDF file of an unedited manuscript that has been accepted for publication. As a service to our customers we are providing this early version of the manuscript. The manuscript will undergo copyediting, typesetting, and review of the resulting proof before it is published in its final form. Please note that during the production process errors may be discovered which could affect the content, and all legal disclaimers that apply to the journal pertain.

Author Manuscript Author Manuscript Author Manuscript Author Manuscript

1. Introduction

TDP2 is a DNA repair enzyme excising 5′-phosphotyrosyl DNA adducts [1–3]. The transient covalent cleavage complexes (TOP2cc) containing 5′-phosphotyrosyl protein-DNA linkages are formed as a part of the normal topoisomerase type II (TOP2α/β) catalytic cycle during DNA relaxation, catenation/decatenation and knotting/unknotting [4]. When treated with TOP2 inhibitors (poisons), the TOP2-DNA cleavage complexes (TOP2ccs) stall as they are prevented from undergoing their final reversal reaction, restoring intact DNA and releasing free TOP2 [4, 5]. Among TOP2 poisons are ETP, mitoxantrone and amsacrine [4]. Stalled TOP2ccs ultimately result in double-stranded DNA breaks. TDP2's primary activity is to excise TOP2 from the DNA 5′- end by catalyzing the hydrolysis of the covalent bond between the DNA phosphate and TOP2 catalytic tyrosine hydroxyl groups [1–3].

Because TDP2 drives resistance to widely used clinical TOP2 poisons[1, 6, 7], it is a legitimate medicinal target. This is supported by elevated sensitivity of TDP2 knockout cells to anticancer TOP2 poisons [1, 6, 7]. Tumors with dysregulations in DNA damage checkpoint (e.g. through ATM mutations) or homologous recombination and non-homologous end-joining deficiencies makes them attractive candidates to treatment with TDP2 and TOP2 inhibitor combinations [8–10]. Based on the viability of TDP2 knockout cells [1, 11] and mice [9], general toxicity is not expected from specific TDP2 inhibitors [9]. TDP2 inhibitors may also be valuable probes to study the role of TDP2 in DNA damage response mediation and as antiviral agents [12–14].

To date several chemical classes have been identified as TDP2 inhibitors: deazaflavins and toxoflavins [15], isoquinoline-1,3-diones [16], furoquinolinedione [17], indenoisoquinolines [18] and NSC111041 [19]. Deazaflavins stand out because of their potency at nanomolar concentration, selectivity for human TDP2 (hTDP2), evidence for targeting cellular TDP2 and crystal structure of the drugs in complex with TDP2 [20, 21]. In a recent report we described new TDP2 inhibitors based on the deazaflavin pharmacophore [22].

Here we evaluate two representative members of deazaflavin subtypes, ZW-1288 and ZW-1231 (Figure 1). We compare the activity profile of these new analogues to the parent compound SV-5-153 and outline general direction for future optimization.

2. Material and Methods

2.1. Media and growth conditions

DT40 cells were cultured in RPMI1640 medium supplemented with L-glutamine, 1% chicken serum, 50 μM β-mercaptoethanol, 10% fetal bovine serum, penicillin, and streptomycin. DU145 and CCRF-CEM cells were cultured in DMEM medium supplemented with 10% fetal bovine serum, penicillin, and streptomycin.

2.2. Recombinant TDP2 assay

TDP2 reactions were carried out as described previously [2] with the following modifications. The 18-mer single-stranded oligonucleotide DNA substrate (TY18, ^{32}P-cordycepin-3′-labeled) was incubated at 1 nM with 25 pM recombinant human TDP2 in the

Author Manuscript Author Manuscript Author Manuscript Author Manuscript

absence or presence of inhibitor for 15 min at room temperature in a buffer containing 50 mM Tris-HCl, pH 7.5, 80 mM KCl, 5 mM MgCl2, 0.1 mM EDTA, 1 mM DTT, 40 μg/mL BSA, and 0.01% Tween 20. Reactions were terminated by the addition of 1 volume of gel loading buffer [99.5% (v/v) formamide, 5 mM EDTA, 0.01% (w/v) xylene cyanol, and 0.01% (w/v) bromophenol blue]. Samples were subjected to a 16% denaturing PAGE with multiple loadings at 12-min intervals. Gels were dried and exposed to a PhosphorImager screen (GE Healthcare). Gel images were scanned using a Typhoon FLA 9500 (GE Healthcare), and densitometry analyses were performed using the ImageQuant software (GE Healthcare).

2.3. Whole cell extract (WCE) TDP2 assay

DT40 knockout cells (1×10^7) for TDP2 ($TDP2^{-/-}$) complemented with human TDP2 (hTDP2) were collected, washed, and centrifuged. Cell pellets were then resuspended in 100 μL of CellLytic M cell lysis reagent (SIGMA-Aldrich C2978). After 15 min on ice, lysates were centrifuged at 12,000 g for 10 min, and supernatants were transferred to a new tube. Protein concentrations were determined using a Nanodrop spectrophotometer (Invitrogen), and whole cell extracts were stored at −80 °C. The TY18 DNA substrate was incubated at 1 nM with 5 μg/mL of whole cell extracts in the absence or presence of inhibitor for 15 min at room temperature in the LMP2 assay buffer. Reactions were terminated by the addition of 1 volume of gel loading buffer [99.5% (v/v) formamide, 5 mM EDTA, 0.01% (w/v) xylene cyanol, and 0.01% (w/v) bromophenol blue]. Samples were subjected to a 16% denaturing PAGE with multiple loadings at 12-min intervals. Gels were dried and exposed to a PhosphorImager screen (GE Healthcare). Gel images were scanned using a Typhoon FLA 9500 (GE Healthcare), and densitometry analyses were performed using the ImageQuant software (GE Healthcare).

2.4. Recombinant TDP1 assay

A 5′-[32P]-labeled single-stranded DNA oligonucleotide containing a 3′-phosphotyrosine (N14Y) [23] was incubated at 1 nM with 10 pM recombinant TDP1 in the absence or presence of inhibitor for 15 min at room temperature in WCE buffer (see above and Figure 3A). When indicated, parallel reactions were performed in a buffer containing 50 mM Tris HCl, pH 7.5, 80 mM KCl, 2 mM EDTA, 1 mM DTT, 40 μg/mL BSA, and 0.01% Tween-20 [2]. Reactions were terminated by the addition of 1 volume of gel loading buffer [99.5% (v/v) formamide, 5 mM EDTA, 0.01% (w/v) xylene cyanol, and 0.01% (w/v) bromophenol blue]. Samples were subjected to a 16% denaturing PAGE with multiple loadings at 12-min intervals. Gels were dried and exposed to a PhosphorImager screen (GE Healthcare). Gel images were scanned using a Typhoon FLA 9500 (GE Healthcare), and densitometry analyses were performed using the ImageQuant software (GE Healthcare).

2.5. Molecular Modeling

Deazaflavins SV5-153, ZW-1231, and ZW-1288 were docked into the hTDP2. The hTDP2 model was built with SWISS-MODEL [24] using mTDP2 structure as a template. The mTDP2 crystal structure (PDB: 4GZ1) was trimmed by removing one of the TDP2 monomer chains, bound DNA, magnesium ions, and water oxygen atoms [21]. The trimmed mTDP2 structure and hTDP2 sequence (UniProtKB - O95551) were submitted to SWISS-

Author Manuscript Author Manuscript Author Manuscript Author Manuscript

MODEL for homology modeling. The hTDP2 structure was further geometry-optimized MacroModel [25] using AMBER* force field with 300 iterations of Steepest Descent (SD) minimization. The ligand structures were prepared in Maestro [26] and geometry-optimized in MacroModel using MMFFs force field with 2500 iteration of Polak-Ribier Conjugate Gradient (PRCG) minimization. The docking of the active TDP2 inhibitors was performed with Glide [27] using Extra Precision setting [28]. The grid for docking was set to cover the catalytic site and DNA binding channel.

2.6. Evaluation of cytotoxicity and synergy

Drug cellular sensitivity was measured as previously described [10]. Briefly, cells were seeded (500 cells/well for DT40; 2000 cells/well for DU145 or CCRF-CEM) into 96-well white plate (PerkinElmer) and continuously exposed to various drug concentrations for 72 hours in triplicate in 100 μl of medium. Cell viability was determined at 72 hours by adding 50 μl of ATPlite solution (ATPlite 1-step kit, PerkinElmer). After 5 min incubation, luminescence was measured on an EnVision Plate Reader (PerkinElmer). The ATP level in untreated cells was defined as 100% percent and viability of treated cells was defined as (ATP level of treated cell/ ATP level of untreated cells) x100. Synergism was assessed with CompuSyn software (http://www.combosyn.com Paramus, NJ).

2.7. Determination of intracellular ETP levels in DT40 cells treated with ETP and TDP2 inhibitors

DT40 cells were cultured in RPMI-1640 medium supplemented with 10% fetal bovine serum, 1% chicken serum, 10^{-5} mol/L β-mercaptoethanol and 1% penicillin-streptomycin. The culture medium was renewed every 2 to 3 days, and the non-adherent cells were maintained between 2×10^5 and 2×10^6 cells/mL in a humidified atmosphere of 5 % CO2 at 37 °C during sub-culturing. For drug treatments, the cells were prepared at a density of 2×10^4 cells/mL and aliquoted into 12 mL in each flask. The flasks were then either treated with ETP at a concentration of 0.15 μM alone or in combination with TDP2 inhibitors of different concentrations for 72 hours. A flask treated with DMSO only was done in parallel as control. All experiments were repeated at least three times. At the end of drug treatments, 1 mL of cells suspension from each flask was collected and cells counting was performed using the Beckman Coulter Vi-CELL XR cell viability analyzer with Trypan Blue Dye exclusion test. Another 10 mL aliquot of cells suspension from each flask was collected and spun down at 200 ×g. The medium was discarded, and the cells pellets were washed three times by re-suspending and spinning down with 1 mL DPBS. After discarding the DPBS, the cells pellets were lysed, and protein precipitated by adding 75 μL of methanol to each vial. The lysed samples were stored at −80 °C until analyzed with LC/MS/MS for intracellular ETP levels.

3. Results

3.1. Recombinant human TDP2 (hTDP2) inhibition

To gauge their *in vitro* hTDP2 inhibitory potency against the recombinant enzyme, the two novel deazaflavins were tested in comparison with SV-5-153 (Figures 1 & 2). TDP2-catalyzed cleavage reactions were carried out with a ^{32}P-labeled DNA oligonucleotide

Author Manuscript Author Manuscript Author Manuscript Author Manuscript

bearing 5′-phosphotyrosyl group [2]. All three compounds inhibited hTDP2 consistent with earlier findings [22]. Their IC_{50} values were within nanomolar range: 81 nM for SV-5-153, 275 nM for ZW-1231, and 102 nM for ZW-1288.

3.2. Cross-resistance of hTDP2 L313H and mTDP2 to deazaflavins

We previously demonstrated that mouse TDP2 (mTDP2) is resistant to SV-5-153, and that H323 of mTDP2 (L313 hTDP2) is a key residues responsible for the resistance [29]. To test whether such trait is carried over to ZW-1231 and ZW-1288, we tested for inhibition of hTDP2 L313H single-point mutant and mTDP2 (Figure 2). All three compounds inhibited hTDP2 L313H with lower efficiency than observed for recombinant hTDP2, with IC_{50}'s of 5.2 μM for SV-5-153, 4.6 μM for ZW1231 and 5.8 μM for ZW-1288. This is equivalent to 17–64-fold resistance of the single point mutant L313H over WT enzyme. In addition, none of the three deazaflavins were capable of inhibiting mTDP2 at concentrations up to 111 μM to a level sufficient for establishing IC50 (Figure 2C). These findings point to the common and selective mechanism of molecular inhibition among the deazaflavins.

3.3. Inhibition of native TDP2 activity in WCE and selectivity for TDP2 versus TDP1

While confirming the *in vitro* potency of SV-5-153, ZW-1231, and ZW-1288, it is important to inquire about the drug's ability to target the enzyme in its physiological environment when other cellular proteins are present. To that effect, TDP2 cleavage reactions were carried out with whole cell extract (WCE) from hTDP2-complemented DT40 knockout cells ($TDP2^{-/-}$) [7] (Figure 3A). Lacking or significantly diminished potency would indicate depletion of the pool of drug through non-specific interactions or differential folding and post-translational modification of hTDP2 in the context of cellular extract. Notably, all three deazaflavins, SV-5-153, ZW-1231 and ZW-1288 inhibited the TDP2 in WCE with 28, 89, and 96 nM IC_{50}'s, respectively. Hence the potency of the novel deazaflavins is retained and even slightly enhanced in nuclear extracts demonstrating their activity against cellular TDP2.

All three compounds were also tested against recombinant hTDP1. None showed detectable activity (Figure 3B). We conclude that the novel deazaflavins ZW-1231 and ZW-1288 selectively inhibit human TDP2 (hTDP2) both in the context of the recombinant enzyme and in nuclear extracts.

3.4. Molecular docking and interactions of ZW-1231, ZW-1288 and SV-5-153 with human TDP2

To assess the molecular interactions of the new deazaflavin derivatives with hTDP2, we constructed a deazaflavin binding model using *in silico* docking. We employed homology modeling and constructed hTDP2 structure using the published mTDP2 as template, based on the conservation between the two proteins [21, 29]. The assumption of mTDP2 suitability as a homology modeling template is borne out by our observation that mTDP2 enzymatic performance and responsiveness to inhibitors can be made to mimic that of hTDP2 with few key mutations in the relative proximity of the catalytic site [29]. Both ZW-1231 and ZW-1288 were found to form complexes with TDP2 similar to SV-5-153. Figure 4 shows the drugs bound to the DNA binding channel adjacent to the site of tyrosyl phosphoester cleavage, forming hydrophobic contacts with L313 and polar contacts to R366. Together

Author Manuscript Author Manuscript Author Manuscript Author Manuscript

these results are consistent with our biochemical findings demonstrating the similarity between the two novel deazaflavins ZW-1231 and ZW-1288 with SV-5-153 and the cross-resistance of the L313H mutant.

3.5. Synergistic activity of the deazaflavins with ETP beyond TDP2 and Mre11

Because we previously reported that SV-5-153 lacks inherent toxicity while enhancing the antiproliferative action of ETP [29], we assessed ZW-1231 and ZW-1288 as single agents. Figure 5 shows that ZW-1288, like SV-5-153 does not show significant single-agent cytotoxicity in the 3 cancer cell lines examined, chicken lymphoblast DT40, human leukemia CCRF-CEM and human prostate carcinoma DU145 cells. However, ZW-1231 exhibited cytotoxicity with GI50 at low micromolar levels. The characteristic 50% growth inhibition (GI_{50}) values are 49.4 μM (ZW-1288), >100 μM (SV-5-153) and 6.5 μM (ZW-1231) in DT40 cells, 22.2 μM (ZW-1288), 24.3 μM (SV-5-153) and 6.1 μM (ZW-1231) in CCRF-CEM cells and 52.9 μM (ZW-1288), 85.7 μM (SV-5-153) and 8.4 μM (ZW-1231) in DU145 cells. These results demonstrate that ZW-1288, which has improved cellular penetration compared to SV-5-153 [22] exhibits limited single-agent cytotoxicity in three cancer cell lines from different tissues of origin. The cytotoxicity of ZW-1231 suggests that this derivative has an off-target effect beyond TDP2. Thus, ZW-1288 was chosen to carry out further drug combination studies.

First, we evaluated ZW-1288 in combination with the TOP2 poison ETP. Synergistic activity of ZW-1288 with ETP was observed in DT40 cells (Figure 6A) at concentrations where ZW-1288 exerted no cytotoxicity on its own. We also tested the combination in DT40 TDP2-KO cells (Figure 6B), and found that ZW-1288 maintained strong synergy. This result demonstrates that ZW-1288 can act independently of TDP2. To determine whether a secondary target of ZW-1288 could be the endonuclease Mre11, which has been implicated in the repair of TOP2cc independently of TDP2 [30–32], we tested the combination of ZW-1288 and ETP in isogenic Mre11-deficient DT40 cells (DT40 $MRE11^{-/H129N}$) [33]. Figure 6C shows that the synergy with ETP was maintained in Mre11-deficient cells, indicating that ZW-1288 has additional cellular target(s) beyond TDP2 and Mre11.

Dose-response curves for the ETP/ZW-1288 combination treatment are plotted side by side with those of SV-5-153 in Figure 6. The dose response curves show greater incline for the ETP/ZW-1288 combination compared to ETP/SV-5-153, indicating stronger synergistic interactions for ZW-1288 (Figure 6). The results of the drug combination analyses of the dose response data (Figure 6A–C, left panels) are presented in form of Combination Index (CI) vs. Fraction Affected (Fa) plots in the right panels of Figures 6A–C. CI values below 1 are indicative of synergism. The CI-Fa plots demonstrate that majority of data points representing ETP/ZW-1288 drug combination lie in the area of strong synergism (CI value of around 0.3). The synergism of ZW-1288 with ETP was found consistently greater than for SV-5-153 (Figure 6, right panels).

To determine whether the synergistic effect of ZW-1288 with ETP was selective for ETP, we tested ZW-1288 in combination with the TOP1 inhibitor camptothecin (Figure 7A) and the PARP inhibitor olaparib (Figure 7B). In both cases no amplification of toxicity was

Author Manuscript Author Manuscript Author Manuscript Author Manuscript

observed, indicating that the synergistic activity of ZW-1288 with ETP is not observed across drugs with other mechanisms of action.

To expand our findings to other TOP2 poisons and cell lines, ZW-1288 was tested in combination with mitoxantrone and ETP in human CCRF-CEM leukemia and DU145 prostate cancer cell lines (Figures 7C–F). ZW-1288 was found to synergize with both ETP and mitoxantrone. In all cases with exception of the ZW-1288-mitoxantrone combination in DU145 cells (Figure 7G), a notable dose-dependent potentiation of TOP2 inhibitors was observed. As evident from increased incline of the dose response curves corresponding to increase in toxicity of ETP with increasing concentration of ZW-1288. Together, these results show that ZW-1288 and SV-5-153 synergizes the activity of TOP2 poisons across cell lines, and that this effect is likely not solely due to TDP2 inhibition.

3.6. Intracellular ETP levels in cells treated with ZW-1288 and SV-5-153

To assess whether the effect of deazaflavins could be due to increased intracellular ETP levels [34], DT40 cells were treated with ETP in combination with ZW-1288 or SV-5-153. After treatment cells were counted using the Beckman Coulter Vi-CELL XR cell viability analyzer with Trypan Blue Dye exclusion test, lysed and analyzed with LC/MS/MS for intracellular ETP levels. The results are presented in Figure 8. The parent compound SV-5-153 had no effect of either toxicity or intracellular ETP level at 1 μM. While it boosted ETP concentration in cells 8-fold at 3 μM, it produced less than 10% increase in ETP-induced cell death from 68% at 1 μM to 76% at 3 μM of SV-5-153. Nearly 5-fold increase relative to control in ETP level was observed at 1 μM of ZW-1288, which coincided with 92% cell death. At 3 μM, ZW-1288 increased ETP concentration nearly 7-fold with 97% cell death. These results show that both SV-5-153 and ZW-1288 increase ETP cellular levels, with ZW-1288 being more potent than SV-5-153. Yet, the cytotoxicity increase was not tightly correlated with the ETP uptake, suggesting that the enhancing effect of the deazaflavins is not simply due to enhanced ETP concentration.

4. Discussion

Our study focuses on two derivatives of the lead deazaflavin compound SV-5-153. These new compounds were prepared as described [35] and designed to improve cellular membrane penetration and medicinal properties of SV-5-153 and its published derivatives [36]. For this purpose, the tetrazole moiety was replaced by the p-hydroxy with the additional aromatic substitutions [35]. We selected two representative members of the newly emerged subtypes [35] for detailed biochemical and cellular evaluation, the N-3 substituted derivative ZW-1288 and the N-10 phenyl ring modified analogue ZW-1231 (Figure 1). Biochemical evaluation of ZW-1231 and ZW-1288 alongside SV-5-153 confirmed that these chemical modifications have no detrimental effect of TDP2 inhibitory potency of the drugs, and that both analogues are on par with the parent deazaflavin when it comes to disrupting TDP2-mediated hydrolysis. We also show they remain inactive against TDP1 (Figures 2 & 3). The two new deazaflavins ZW-1288 and ZW-1231 maintain inhibitory potency against TDP2 in WCE, demonstrating that very little or no drug sequestration occurs through non-

Author Manuscript Author Manuscript Author Manuscript Author Manuscript

specific binding to the bulk of other cellular proteins and points to the activity of the drugs against human TDP2 in cellular environment.

We previously established that mouse TDP2 (mTDP2) is resistant to SV-5-153 [20]. Further analysis of single-point mutants revealed a number of amino acid residues that contribute to mTDP2 resistance to deazaflavins. Among these residues, the single most significant contributor to the resistance is H323 of mTDP2 (L313 in hTDP2). This residue is distant from the catalytic site of TDP2, mTDP2 H323-Cα – Mg^{2+} 13.0 Å (PDBID: 4GZ1) [21] and it is located along the DNA binding channel in the proximity of +2 nucleobase upstream of 5′-phosphotyrosyl cleavage site (see Figure 4). Furthermore, we established that L313H mutation in hTDP2 confers significant resistance to SV-5-153 [29]. The crystallographic studies revealed that SV-5-153 binds to TDP2 on top of L313 forming Van der Waals interactions with this residue [36]. ZW-1288 and ZW-1331 were engineered with significant deviations from the parent SV-5-153 with the addition of either a bulky hydrophobic benzyl moiety to N-10 phenyl ring in ZW-1231 or addition of an aromatic ring to N-3 in ZW-1288 (see Figure 1). Because such chemical modifications can substantially change binding site and mode, in addition to evaluation of naïve hTDP2 inhibitory potency, we assessed performance of these analogues against hTDP2 L313H and mTDP2 (Figure 2). As in the case of SV-5-153, both ZW-1331 and ZW-1288 are 17–59 times less potent against hTDP2 L313H, and mTDP2 is highly resistant to all three drugs (Figures 2B–D). These findings indicate preservation of the binding site in proximity of the key residue L313 of hTDP2 among the three deazaflavins.

Our analyses of the binding of SV-5-153, ZW-1231 and ZW-1288 with hTDP2 (Figure 4) by molecular docking placed SV-5-153 in the same substrate binding groove of TDP2 found by crystallography [36], although the preferred orientation of the SV-5-153 core was perpendicular to the DNA binding channel (Figure 4A). Nevertheless, the interaction with the key residue L313 was consistent with the importance of that residue for drug inhibitory activity (Figures 3 & 4). Docking of ZW-1231 replicated the modeled pose of SV-5-153 polycyclic core (Figure 4A and 4B) with the newly introduced benzyl group completely covering the surface area of L313. In the case of ZW-1288 a different hypothetical pose of the inhibitor core was favored by docking algorithm with the fused tricyclic motif arranged along the DNA binding channel and the N-3 phenyl substituent placed in contact with L313. The docked poses of all three drugs have predicted interaction with R366, one of the TDP2 residues responsible for binding substrate DNA phosphodiester backbone. Therefore, the combination of biochemical evaluation and docking results satisfactorily demonstrate that despite chemical structural changes with introduction of new substituents, the binding site and overall mode of inhibition are preserved for the two new deazaflavin derivatives ZW-1231 and ZW-1288 [36].

It is expected that the specific TDP2 inhibitors would be largely non-toxic based on the dispensability of TDP2 for cell survival [2, 7, 37] and murine development [11]. Although ZW-1231 exhibited toxicity at concentrations above 50 μM, ZW-1288 remained largely non-toxic at concentrations up to 100 μM mirroring the behavior of SV-5-153 (Figure 5). It is worth noting that both ZW-1231 and ZW-1288 surpass SV-5-153 in cell permeability with

Author Manuscript Author Manuscript Author Manuscript Author Manuscript

PAMPA effective permeability coefficients (10^{-6} cm/s) of 0.6, 0.1 and 0.003, respectively [22].

Selective TDP2 inhibitors should only potentiate the cytotoxicity of TOP2 poisons (such as ETP) as TDP2 is a key pathway for removing trapped TOP2 cleavage complexes [2, 4, 11, 20, 21, 38]. Accordingly, we found that ZW-1288 potentiates the action of ETP in three cancer cell lines examined, chicken lymphoma DT40, human prostate carcinoma DU145 and leukemia CCRF-CEM cells (Figures 6 and 7C–G). Notably, ZW-1288 had no impact on the cytotoxicity of the TOP1 inhibitor camptothecin or the PARP-1 inhibitor olaparib (Figure 7A and 7B), consistent with the lack of any TDP1 inhibition potency for ZW-1288 (Figure 3B). However, we also observed synergy between ZW-1288 and ETP in DT40 cells lacking either TDP2 or expressing the nuclease-impaired MRE11$^{-/H129N}$ cells (Figure 6B and 6C). These observations indicate that the cellular effect of the deazaflavins revolves around such TOP2 inhibitors as ETP and mitoxantrone.

Despite having a bulky aryl substituent at N-3 position and potentially different orientation of pharmacophore within the binding site (Figure 4), ZW-1288 behaves similarly to parent lead SV-5-153 both *in vitro* inhibition of TDP2 (Figure 2A and 2C) and in its interaction with TOP2 poisons in cellular culture (Figures 6 and 7).

While our present work was in progress, the property of deazaflavins to affect ETP intracellular concentration arguably through influx/efflux has been reported [34]. Here we confirm that the deazaflavins SV-5-153 and ZW-1288 enhance the accumulation of intracellular ETP. However, the synergistic action of the deazaflavins in combination with ETP is probably more complex. As seen in Figure 8, SV-5-153 at 3 μM concentration promotes over 8-fold increase in intracellular ETP concentration, which coincides with only ~10% increase in cell death, while SV-5-153 at 1 μM fails to affect either parameter. In the case of ZW-1288, a more modest increase in intracellular ETP at 1 μM of ZW-1288 coincides with much stronger increase in cytotoxic effect than for SV-5-153 at 3 μM. This leads us to conclude that while the deazaflavin effect on ETP cellular concentration is a contributing factor to the observed synergy, the lack of correlation between intracellular ETP concentration and cell death in its combinations with SV-5-153 or ZW-1288 is not the sole driving force for this synergy. In addition to TDP2 inhibition, other intracellular activities of deazaflavins might be responsible for such synergistic cooperation with ETP and mitoxantrone as indicated by the results with DT40 TDP2$^{-/-/-}$ or MRE11$^{-/H129N}$ cells.

In summary, our study demonstrates the potential of the deazaflavin series as the most potent TDP2 inhibitors to date and potentiators of TOP2 inhibitors in cells. It also highlights a way forward for the development of monospecific deazaflavin TDP2 inhibitors by selecting drugs that selectively synergize with ETP in TDP2-proficient cells and do not affect ETP cellular uptake. While ZW-1288 appear to selectively affect the response to the TOP2-mediated DNA damage, it would be beneficial to develop a compound that lacks synergistic potential in systems deprived of TDP2 and exerts minimal effect on influx/efflux of ETP.

Author Manuscript Author Manuscript Author Manuscript Author Manuscript

Acknowledgements.

E.K., A.R. and Y.P. are supported by the Intramural Program of the National Cancer Institute, Center for Cancer Research, NIH (Z01-BC-006150). J.X. thanks the Center for Drug Design, University of Minnesota, for financial support. Z.W. acknowledges the support from University of Minnesota's AHC Faculty Research Development Grant (FRD #14.23).

References

[1]. Cortes Ledesma F, El Khamisy SF, Zuma MC, Osborn K, Caldecott KW, A human 5'-tyrosyl DNA phosphodiesterase that repairs topoisomerase-mediated DNA damage., Nature, 461 (2009) 674–678. [PubMed: 19794497]

[2]. Gao R, Huang SY, Marchand C, Pommier Y, Biochemical characterization of human tyrosyl-DNA phosphodiesterase 2 (TDP2/TTRAP): a Mg(2+)/Mn(2+)-dependent phosphodiesterase specific for the repair of topoisomerase cleavage complexes, J Biol Chem, 287 (2012) 30842–30852. [PubMed: 22822062]

[3]. Pommier Y, Huang SY, Gao R, Das BB, Murai J, Marchand C, Tyrosyl-DNA-phosphodiesterases (TDP1 and TDP2), DNA repair, 19 (2014) 114–129. [PubMed: 24856239]

[4]. Pommier Y, Sun Y, Huang SN, Nitiss JL, Roles of eukaryotic topoisomerases in transcription, replication and genomic stability, Nat Rev Mol Cell Biol, 17 (2016) 703–721. [PubMed: 27649880]

[5]. Nitiss JL, Targeting DNA topoisomerase II in cancer chemotherapy, Nat. Rev. Cancer, 9 (2009) 338–350. [PubMed: 19377506]

[6]. Maede Y, Shimizu H, Fukushima T, Kogame T, Nakamura T, Miki T, Takeda S, Pommier Y, Murai J, Differential and Common DNA Repair Pathways for Topoisomerase I- and II-Targeted Drugs in a Genetic DT40 Repair Cell Screen Panel, Molecular cancer therapeutics, In press (2013).

[7]. Zeng Z, Sharma A, Ju L, Murai J, Umans L, Vermeire L, Pommier Y, Takeda S, Huylebroeck D, Caldecott KW, El-Khamisy SF, TDP2 promotes repair of topoisomerase I-mediated DNA damage in the absence of TDP1, Nucleic Acids Res, 40 (2012) 8371–8380. [PubMed: 22740648]

[8]. Alvarez-Quilon A, Serrano-Benitez A, Lieberman JA, Quintero C, Sanchez-Gutierrez D, Escudero LM, Cortes-Ledesma F, ATM specifically mediates repair of double-strand breaks with blocked DNA ends, Nature communications, 5 (2014) 3347.

[9]. Gomez-Herreros F, Romero-Granados R, Zeng Z, Alvarez-Quilon A, Quintero C, Ju L, Umans L, Vermeire L, Huylebroeck D, Caldecott KW, Cortes-Ledesma F, TDP2-dependent non-homologous end-joining protects against topoisomerase II-induced DNA breaks and genome instability in cells and in vivo, PLoS genetics, 9 (2013) e1003226. [PubMed: 23505375]

[10]. Maede Y, Shimizu H, Fukushima T, Kogame T, Nakamura T, Miki T, Takeda S, Pommier Y, Murai J, Differential and Common DNA Repair Pathways for Topoisomerase I- and II-Targeted Drugs in a Genetic DT40 Repair Cell Screen Panel, Mol. Cancer Ther, 13 (2014) 214–220. [PubMed: 24130054]

[11]. Gomez-Herreros F, Schuurs-Hoeijmakers JH, McCormack M, Greally MT, Rulten S, Romero-Granados R, Counihan TJ, Chaila E, Conroy J, Ennis S, Delanty N, Cortes-Ledesma F, de Brouwer AP, Cavalleri GL, El-Khamisy SF, de Vries BB, Caldecott KW, TDP2 protects transcription from abortive topoisomerase activity and is required for normal neural function, Nature genetics, 46 (2014) 516–521. [PubMed: 24658003]

[12]. Maciejewski S, Ullmer W, Semler BL, VPg unlinkase/TDP2 in cardiovirus infected cells: Re-localization and proteolytic cleavage, Virology, 516 (2018) 139–146. [PubMed: 29353210]

[13]. Virgen-Slane R, Rozovics JM, Fitzgerald KD, Ngo T, Chou W, van der Heden van Noort GJ, Filippov DV, Gershon PD, Semler BL, An RNA virus hijacks an incognito function of a DNA repair enzyme, Proc Natl Acad Sci U S A, 109 (2012) 14634–14639. [PubMed: 22908287]

[14]. Koniger C, Wingert I, Marsmann M, Rosler C, Beck J, Nassal M, Involvement of the host DNA-repair enzyme TDP2 in formation of the covalently closed circular DNA persistence reservoir of hepatitis B viruses, Proc Natl Acad Sci U S A, 111 (2014) E4244–4253. [PubMed: 25201958]

[15]. Raoof A, Depledge P, Hamilton NM, Hamilton NS, Hitchin JR, Hopkins GV, Jordan AM, Maguire LA, McGonagle AE, Mould DP, Rushbrooke M, Small HF, Smith KM, Thomson GJ,

Author Manuscript Author Manuscript Author Manuscript Author Manuscript

Turlais F, Waddell ID, Waszkowycz B, Watson AJ, Ogilvie DJ, Toxoflavins and deazaflavins as the first reported selective small molecule inhibitors of tyrosyl-DNA phosphodiesterase II, J Med Chem, 56 (2013) 6352–6370. [PubMed: 23859074]

[16]. Kankanala J, Marchand C, Abdelmalak M, Aihara H, Pommier Y, Wang Z, Isoquinoline-1,3-diones as Selective Inhibitors of Tyrosyl DNA Phosphodiesterase II (TDP2), J Med Chem, 59 (2016) 2734–2746. [PubMed: 26910725]

[17]. Yu L-M, Hu Z, Chen Y, Ravji A, Lopez S, Plescia CB, Yu Q, Yang H, Abdelmalak M, Saha S, Agama K, Kiselev E, Marchand C, Pommier Y, An L-K, Synthesis and structure-activity relationship of furoquinolinediones as inhibitors of Tyrosyl-DNA phosphodiesterase 2 (TDP2), Eur. J. Med. Chem, 151 (2018) 777–796. [PubMed: 29677635]

[18]. Wang P, Elsayed MSA, Plescia CB, Ravji A, Redon CE, Kiselev E, Marchand C, Zeleznik O, Agama K, Pommier Y, Cushman M, Synthesis and Biological Evaluation of the First Triple Inhibitors of Human Topoisomerase 1, Tyrosyl-DNA Phosphodiesterase 1 (Tdp1), and Tyrosyl-DNA Phosphodiesterase 2 (Tdp2), J. Med. Chem, 60 (2017) 3275–3288. [PubMed: 28418653]

[19]. Kont YS, Dutta A, Mallisetty A, Mathew J, Minas T, Kraus C, Dhopeshwarkar P, Kallakury B, Mitra S, Uren A, Adhikari S, Depletion of tyrosyl DNA phosphodiesterase 2 activity enhances etoposide-mediated double-strand break formation and cell killing, DNA repair, 43 (2016) 38–47. [PubMed: 27235629]

[20]. Marchand C, Abdelmalak M, Kankanala J, Huang SY, Kiselev E, Fesen K, Kurahashi K, Sasanuma H, Takeda S, Aihara H, Wang Z, Pommier Y, Deazaflavin Inhibitors of Tyrosyl-DNA Phosphodiesterase 2 (TDP2) Specific for the Human Enzyme and Active against Cellular TDP2, ACS Chem Biol, 11 (2016) 1925–1933. [PubMed: 27128689]

[21]. Schellenberg MJ, Appel CD, Adhikari S, Robertson PD, Ramsden DA, Williams RS, Mechanism of repair of 5'-topoisomerase II-DNA adducts by mammalian tyrosyl-DNA phosphodiesterase 2, Nat Struct Mol Biol, 19 (2012) 1363–1371. [PubMed: 23104055]

[22]. Kankanala J, Ribeiro CJA, Kiselev E, Ravji A, Williams J, Xie J, Aihara H, Pommier Y, Wang Z, Novel Deazaflavin Analogues Potently Inhibited Tyrosyl DNA Phosphodiesterase 2 (TDP2) and Strongly Sensitized Cancer Cells toward Treatment with Topoisomerase II (TOP2) Poison Etoposide, J Med Chem, 62 (2019) 4669–4682. [PubMed: 30998359]

[23]. Marchand C, Lea WA, Jadhav A, Dexheimer TS, Austin CP, Inglese J, Pommier Y, Simeonov A, Identification of phosphotyrosine mimetic inhibitors of human tyrosyl-DNA phosphodiesterase I by a novel AlphaScreen high-throughput assay, Molecular cancer therapeutics, 8 (2009) 240–248. [PubMed: 19139134]

[24]. Arnold K, Bordoli L, Kopp J, Schwede T, The SWISS-MODEL workspace: a web-based environment for protein structure homology modelling, Bioinformatics, 22 (2006) 195–201. [PubMed: 16301204]

[25]. Schrödinger, Schrödinger Release 2017–4: MacroModel, Schrödinger, LLC, New York, NY, 2017, in, 2017.

[26]. Schrödinger, Schrödinger Release 2017–4: Maestro, Schrödinger, LLC, New York, NY, 2017, in, 2017.

[27]. Schrödinger, Schrödinger Release 2017–4: Glide, Schrödinger, LLC, New York, NY, 2017, in, 2017.

[28]. Friesner RA, Murphy RB, Repasky MP, Frye LL, Greenwood JR, Halgren TA, Sanschagrin PC, Mainz DT, Extra precision glide: Docking and scoring incorporating a model of hydrophobic enclosure for protein-ligand complexes, J. Med. Chem, 49 (2006) 6177–6196. [PubMed: 17034125]

[29]. Marchand C, Abdelmalak M, Kankanala J, Huang SY, Kiselev E, Fesen K, Kurahashi K, Sasanuma H, Takeda S, Aihara H, Wang ZQ, Pommier Y, Deazaflavin Inhibitors of Tyrosyl-DNA Phosphodiesterase 2 (TDP2) Specific for the Human Enzyme and Active against Cellular TDP2, ACS Chem. Biol, 11 (2016) 1925–1933. [PubMed: 27128689]

[30]. Hoa NN, Shimizu T, Zhou ZW, Wang ZQ, Deshpande RA, Paull TT, Akter S, Tsuda M, Furuta R, Tsusui K, Takeda S, Sasanuma H, Mre11 Is Essential for the Removal of Lethal Topoisomerase 2 Covalent Cleavage Complexes, Mol Cell, 64 (2016) 580–592. [PubMed: 27814490]

Author Manuscript Author Manuscript Author Manuscript Author Manuscript

[31]. Aparicio T, Baer R, Gottesman M, Gautier J, MRN, CtIP, and BRCA1 mediate repair of topoisomerase II-DNA adducts, J Cell Biol, 212 (2016) 399–408. [PubMed: 26880199]

[32]. Maede Y, Shimizu H, Fukushima T, Kogame T, Nakamura T, Miki T, Takeda S, Pommier Y, Murai J, Differential and Common DNA Repair Pathways for Topoisomerase I- and II-Targeted Drugs in a Genetic DT40 Repair Cell Screen Panel, Mol Cancer Ther, 13 (2014) 214–220. [PubMed: 24130054]

[33]. Hoa NN, Akagawa R, Yamasaki T, Hirota K, Sasa K, Natsume T, Kobayashi J, Sakuma T, Yamamoto T, Komatsu K, Kanemaki MT, Pommier Y, Takeda S, Sasanuma H, Relative contribution of four nucleases, CtIP, Dna2, Exo1 and Mre11, to the initial step of DNA double-strand break repair by homologous recombination in both the chicken DT40 and human TK6 cell lines, Genes Cells, 20 (2015) 1059–1076. [PubMed: 26525166]

[34]. Komulainen E, Pennicott L, Le Grand D, Caldecott KW, Deazaflavin Inhibitors of TDP2 with Cellular Activity Can Affect Etoposide Influx and/or Efflux, ACS Chem Biol, (2019).

[35]. Ribeiro CJA, Kankanala J, Shi K, Kurahashi K, Kiselev E, Ravji A, Pommier Y, Aihara H, Wang ZQ, New fluorescence-based high-throughput screening assay for small molecule inhibitors of tyrosyl-DNA phosphodiesterase 2 (TDP2), Eur J Pharm Sci, 118 (2018) 67–79. [PubMed: 29574079]

[36]. Hornyak P, Askwith T, Walker S, Komulainen E, Paradowski M, Pennicott LE, Bartlett EJ, Brissett NC, Raoof A, Watson M, Jordan AM, Ogilvie DJ, Ward SE, Atack JR, Pearl LH, Caldecott KW, Oliver AW, Mode of action of DNA-competitive small molecule inhibitors of tyrosyl DNA phosphodiesterase 2, Biochem J, 473 (2016) 1869–1879. [PubMed: 27099339]

[37]. Cortes Ledesma F, El Khamisy SF, Zuma MC, Osborn K, Caldecott KW, A human 5'-tyrosyl DNA phosphodiesterase that repairs topoisomerase-mediated DNA damage, Nature, 461 (2009) 674–678. [PubMed: 19794497]

[38]. Schellenberg MJ, Lieberman JA, Herrero-Ruiz A, Butler LR, Williams JG, Munoz-Cabello AM, Mueller GA, London RE, Cortes-Ledesma F, Williams RS, ZATT (ZNF451)-mediated resolution of topoisomerase 2 DNA-protein cross-links, Science, 357 (2017) 1412–1416. [PubMed: 28912134]

Author Manuscript Author Manuscript Author Manuscript Author Manuscript

Highlights

- Novel deazaflavin derivative ZW-1288 is a potent inhibitor of recombinant and cellular human TDP2.
- ZW-1288 specifically potentiates cytotoxic action of the clinical TOP2 inhibitors etoposide (ETP) and mitoxantrone.
- ZW-1288 surpasses its parent analogue SV-5-153 in synergism with etoposide.
- ZW-1288 does not impact the activity of the topoisomerase I (TOP1) inhibitor camptothecin or the PARP inhibitor olaparib.
- ZW-1288 actively synergizes with etoposide in TDP2 knockout cells, indicating additional cellular targets.

Author Manuscript Author Manuscript Author Manuscript Author Manuscript

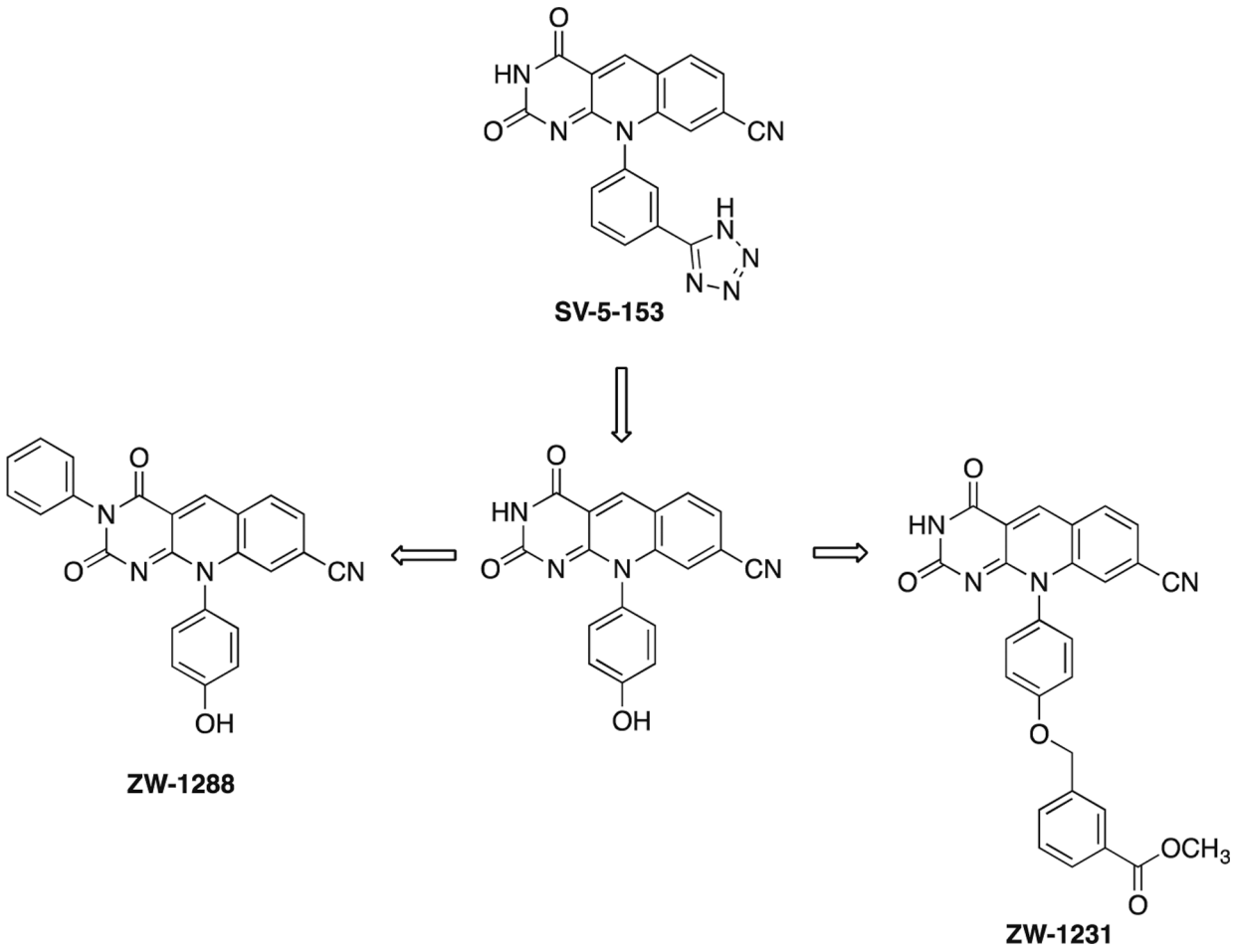

Figure 1.

Derivatization of deazaflavin TDP2 inhibitor SV-5-153: new deazaflavin TDP2 inhibitors are obtained by replacing the tetrazole of the previously reported competitive TDP2 inhibitor SV-5-153 with *p*-hydroxy followed by derivatization of OH (ZW-1231) or NH (ZW1288) groups.

Author Manuscript Author Manuscript Author Manuscript Author Manuscript

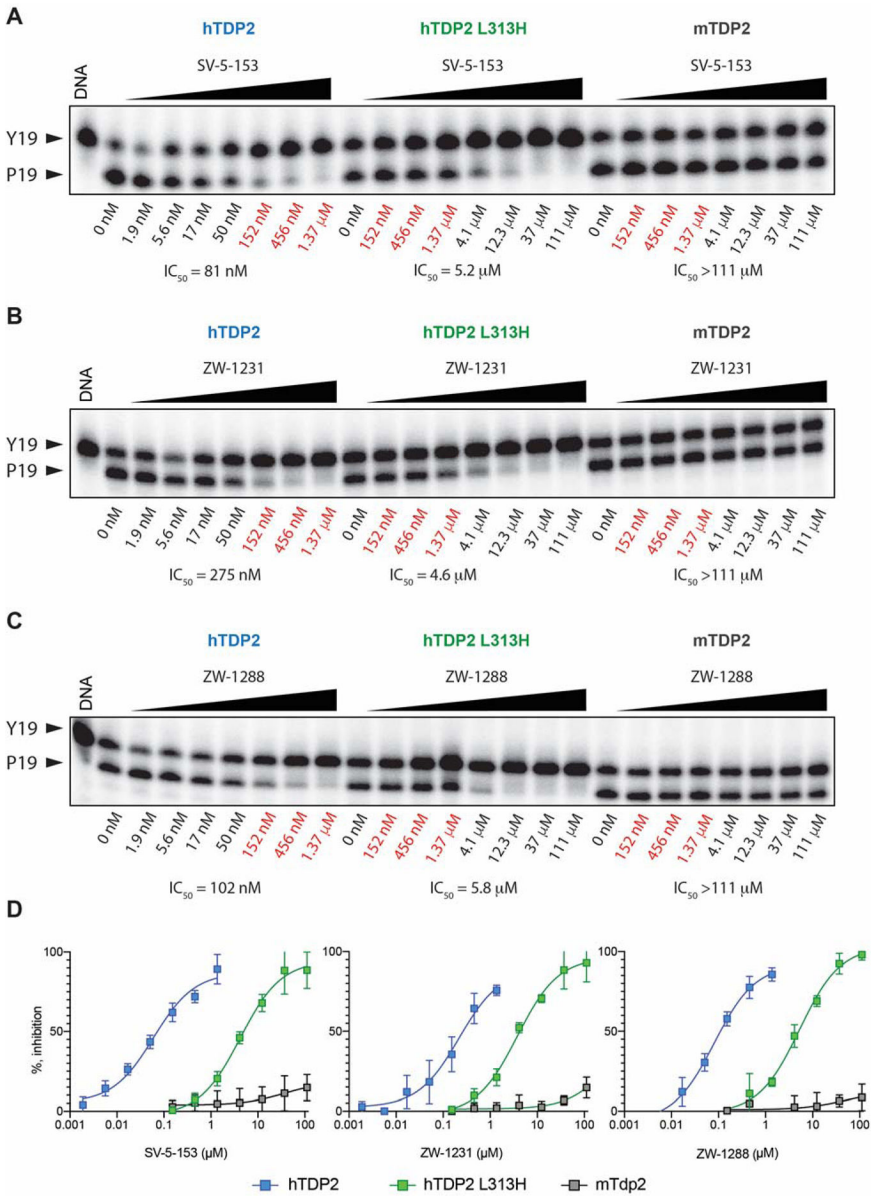

Figure 2.

Representative gel images of TDP2-catalyzed 5′-phosphotyrosyl cleavage reaction in the presence of deazaflavins SV-5-153 (**A**), ZW-1231 (**B**), ZW-1288 (**C**) with respective IC_{50} values reported underneath as a result of gel quantification (**D**) plotted as dose-response curves (n = 3).

Author Manuscript Author Manuscript Author Manuscript Author Manuscript

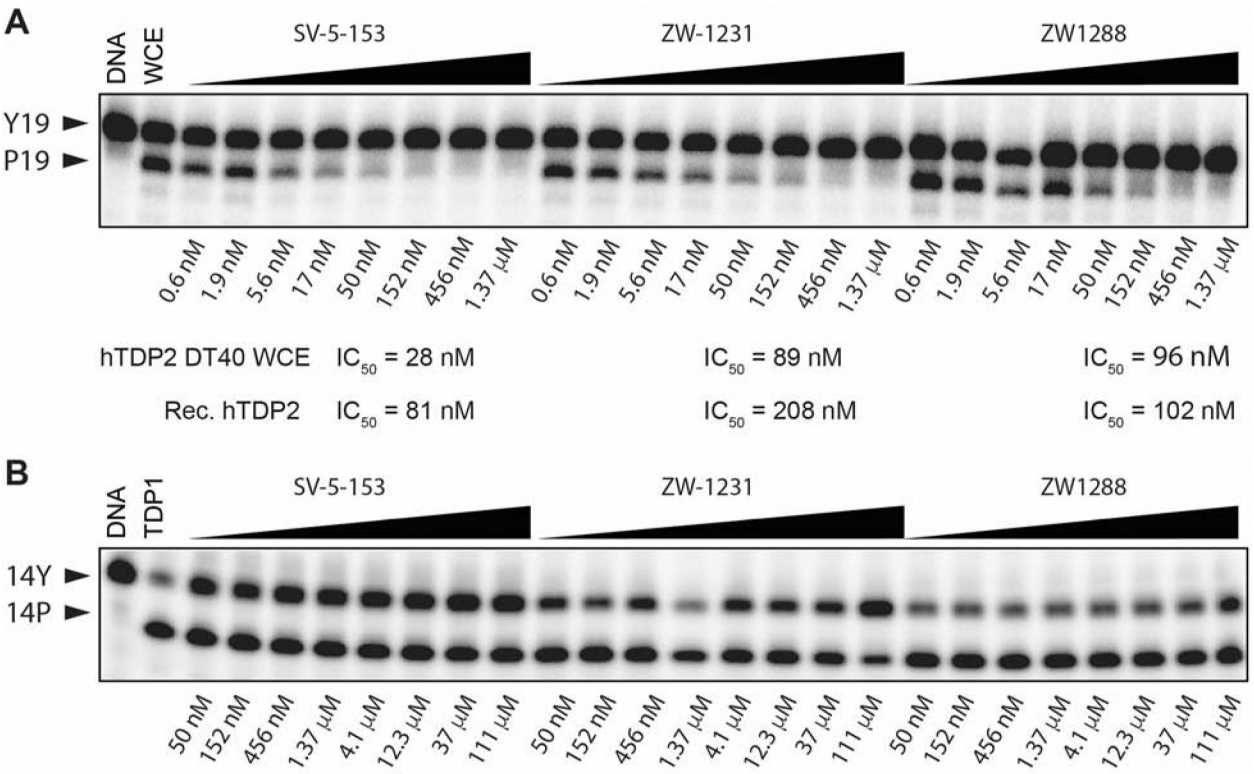

Figure 3.

A. Deazaflavins suppress TDP2-mediated cleavage activity of whole cell extract from hTDP2-complemented DT40 knockout cells (TDP2−/−). Deazaflavins retain nanomolar level of TDP2 inhibitory potency (IC_{50}) against both recombinant TDP2 and WCE. Retention of TDP2 inhibitory potency among deazaflavins suggests that this activity would translate into TDP2 inhibition in vivo and points to limited or absent off target binding. **B**. SV-5-153, ZW-1231 and ZW1288 do not affect TDP1-mediated cleavage of 3′-end DNA lesions.

Author Manuscript Author Manuscript Author Manuscript Author Manuscript

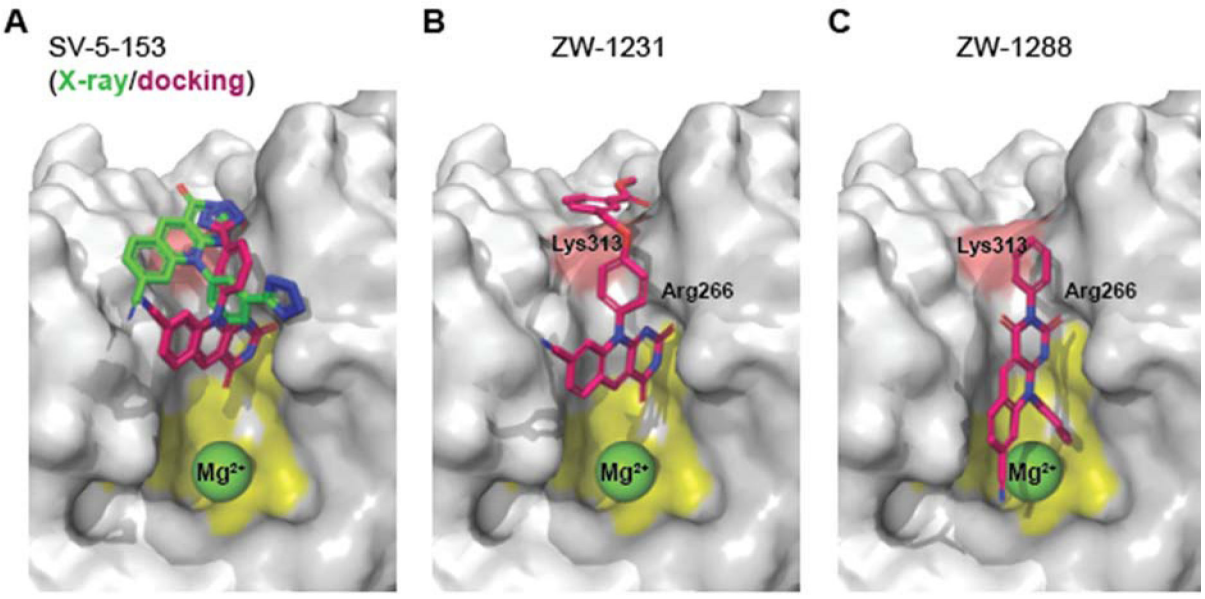

Figure 4.

Comparison of deazaflavin binding modes of SV5-153, hypothetical binding modes with hTDP2 (homology model, grey surface, catalytic residues highlighted in yellow, Lys313 is in pink). **A**. Comparison of the crystallographically established binding mode of SV-5-153 (green, PDBID: 5J3S) and binding mode obtained by docking (red). **B**. Hypothetical binding mode of ZW-1231 (red). **C**. Hypothetical binding mode and ZW-1288 (red). Docking poses of all three ligands show placement of the phenyl ring in close proximity of hTDP2 L313 (pink) explaining the effect of the mutation on inhibitor performance as well as resistance of mouse TDP2 enzyme to the deazaflavins.

Author Manuscript Author Manuscript Author Manuscript Author Manuscript

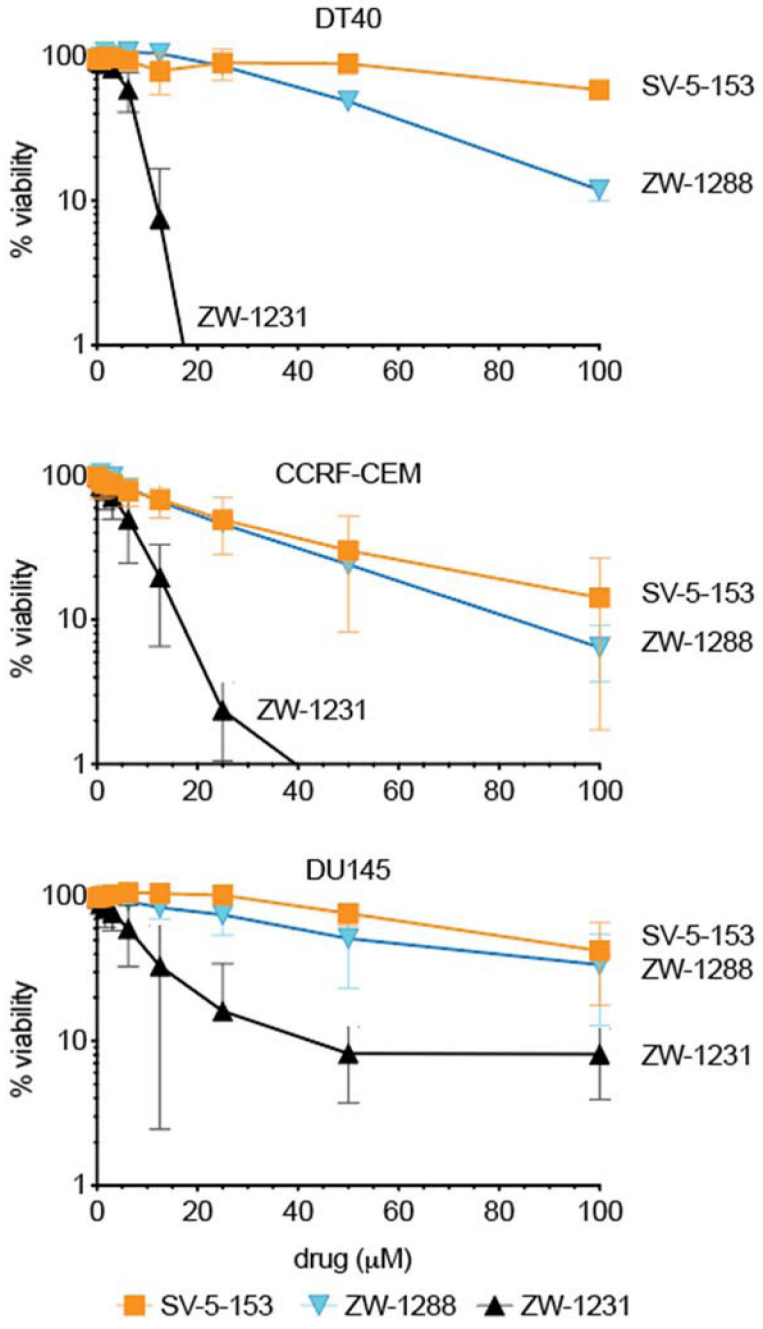

Figure 5.

ZW-1288 shows limited toxicity as single agent. ATPLite cell viability assay of deazaflavins in chicken DT40, as well as human DU145 and CCRF-CEM cells demonstrates that ZW-1231 is cytotoxic as single agent.

Author Manuscript Author Manuscript Author Manuscript Author Manuscript

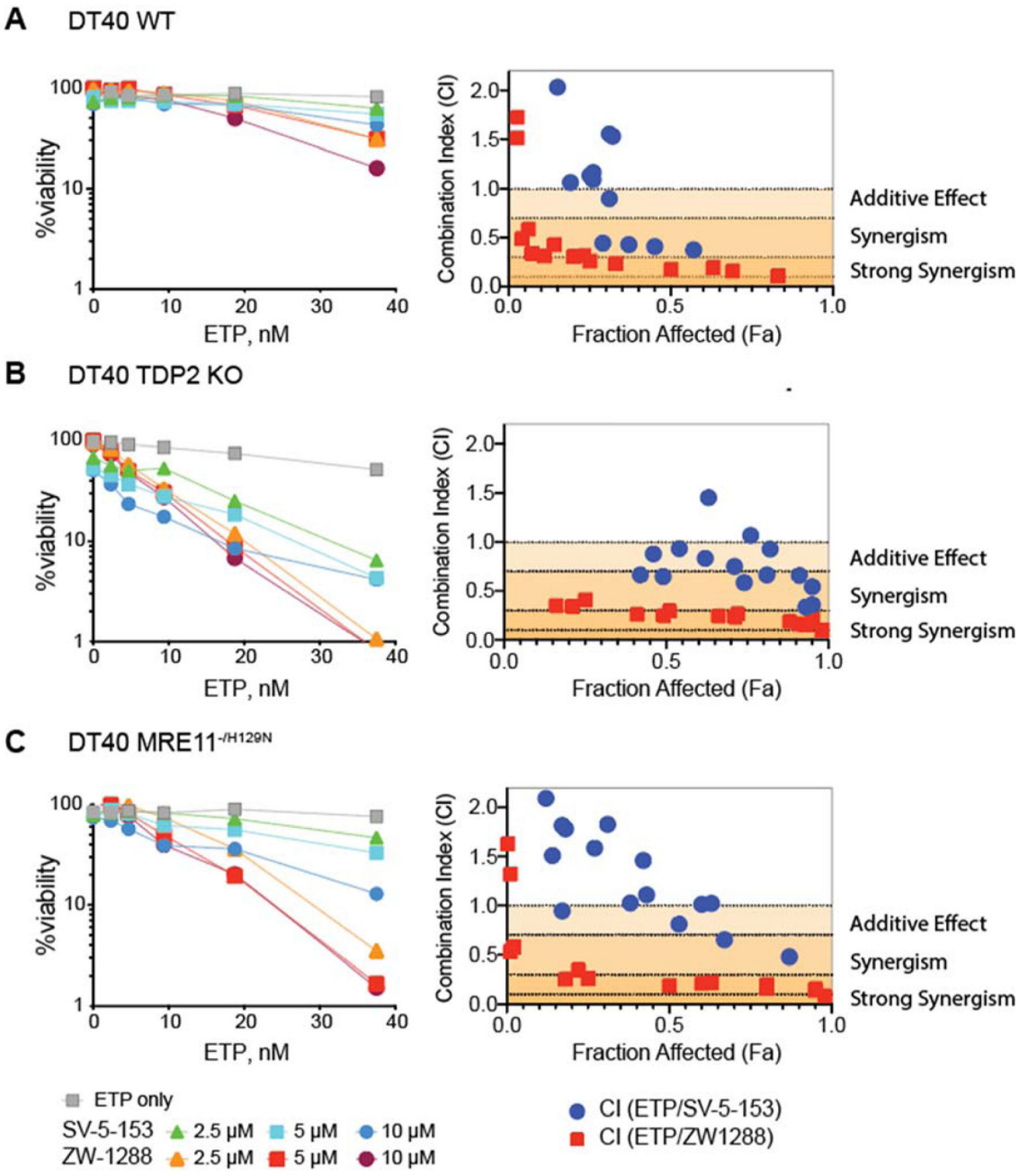

Figure 6.

Potentiation of the cytotoxic action of ETP by deazaflavins S ZW-1288 and SV-5-153 in DT40 WT (**A**), TDP2 KO (**B**) and MRE11-/H129N (**C**). Left panels: dose response curves for combination treatment with ETP and SV-5-153 (green and blue) or ZW-1288 (orange and red). Right panels: combination Index (CI) vs. Fraction Affected (Fa) plot for the dose response graphs in the left panels.

Author Manuscript Author Manuscript Author Manuscript Author Manuscript

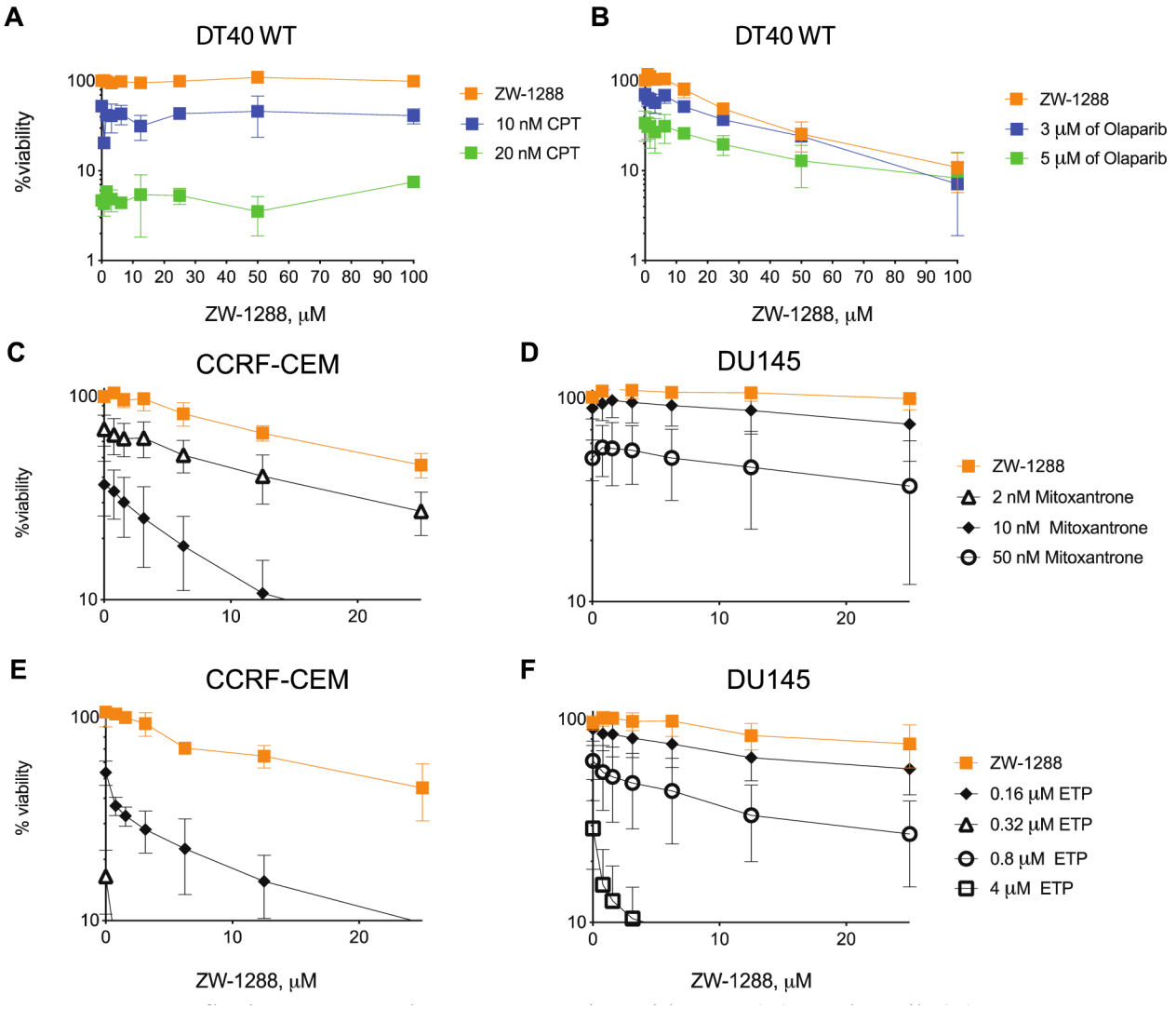

Figure 7.

Deazaflavin ZW-1288 does not synergize with CPT (**A**) or olaparib (**B**). ZW-1288 synergizes with the TOP2 inhibitors ETP and mitoxantrone in CCRF-CEM and DU145 cells (**C**-**F**).

Author Manuscript Author Manuscript Author Manuscript Author Manuscript

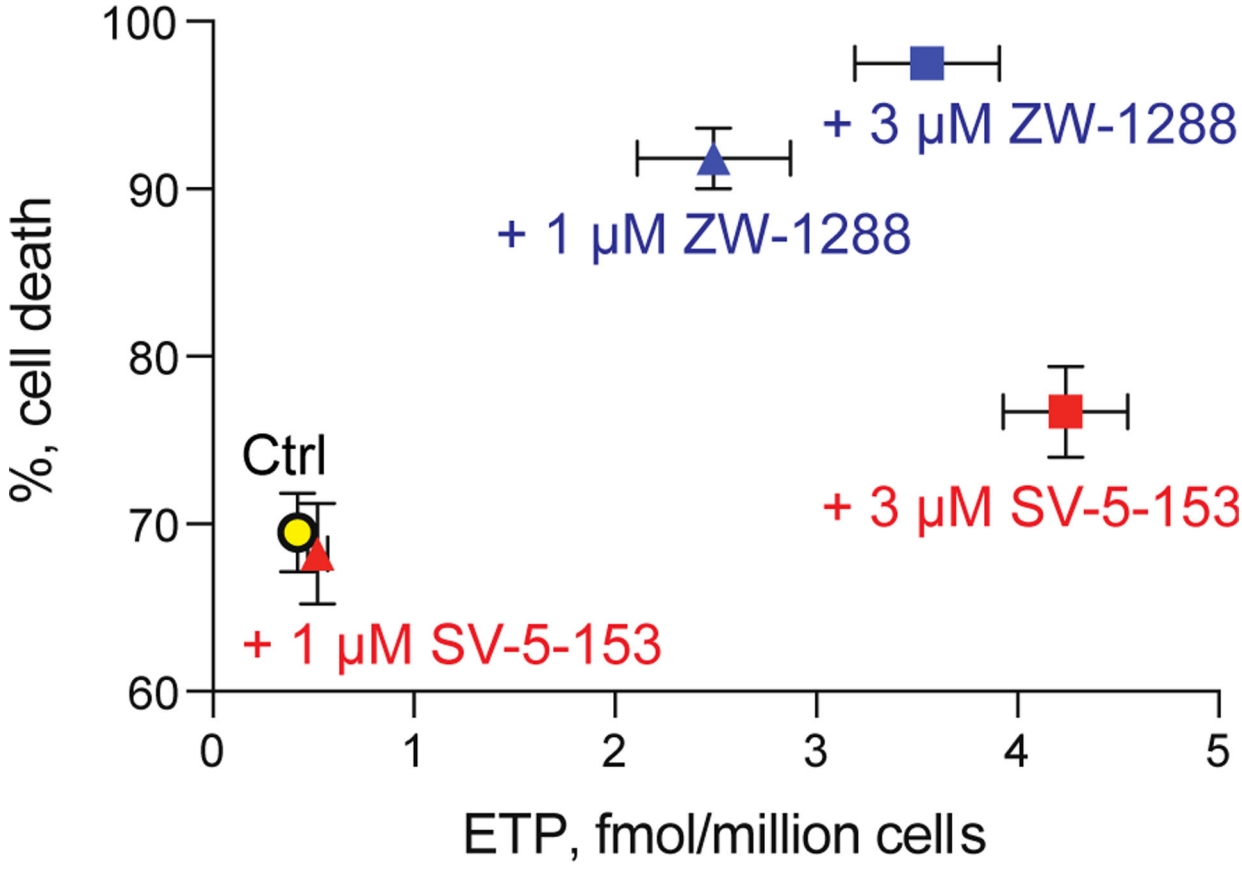

Figure 8.

Effect of SV-5-153 (red) and ZW-1288 (blue) on ETP uptake and relationship with cell viability. DT40 WT cells were treated with 150 nM ETP (circle) or a combination of 150 nM ETP with SV-5-153 (1 μM – red triangle, 3 μM – red square) or a combination of 150 nM ETP with ZW-1288 (1 μM - blue triangle, 3 μM – blue square).